

# TEM study of the mechanism of Ni ion release from Nitinol wires with original oxides

H. Tian<sup>a1</sup>, D. Schryvers<sup>1</sup>, S. Shabalovskaya<sup>2,3</sup> and J. Van Humbeeck<sup>2</sup>

<sup>1</sup> EMAT, University of Antwerp, Groenenborgerlaan 171, B-2020 Antwerp, Belgium

<sup>2</sup> MTM, K. U. Leuven, Kasteelpark Arenberg 44, bus 2450, B-3001 Leuven, Belgium

<sup>3</sup> Ames Laboratory – DOE, Ames, IA 50011, USA

**Abstract.** The surface of commercial Nitinol wires with original oxides and a thickness in the 30-190 nm range was investigated by different state of art TEM techniques. The oxide surface layer was identified as a combination of TiO and TiO<sub>2</sub> depending on the processing of the wire. Between the core of the wires and the oxidized surface, an interfacial Ni<sub>3</sub>Ti nanolayer was observed while Ni nanoparticles are found inside the original oxide. The particle sizes, their distribution in the surface and the Ti-O stoichiometry were deduced from the analysis of the obtained data. Molecular dynamics calculations performed for evaluation of the stability of Ni particles relative to the atomic state revealed that a pure Ni particle has a lower energy than free Ni atoms inside the TiO<sub>2</sub> lattice. The obtained results are discussed with respect to surface stability and Ni release in the human body.

## 1. Introduction

Nitinol is a biomaterial of choice for versatile medical applications due to its unique mechanical properties and a higher compatibility with living tissues in terms of mechanical properties when compared with traditional medical alloys. Moreover, Ti based oxides are formed on Nitinol surfaces naturally providing good biocompatibility. However, there is a possibility of Ni surface enrichment and following release in the human body. This possibility is becoming a reality when the Nitinol surface is not prepared appropriately. A growing number of evidences of systemic allergic responses to Nitinol implants [1-5] in Ni sensitive patients is alarming. This implies that, at present, our knowledge on Ni sources in the alloy product as well as the mechanism of Ni release into the body is not satisfactory.

The goal of the present ongoing study was to evaluate the surface conditions of several superelastic Ni-Ti wires with original surface oxide resulting from processing, and to identify the sources of Ni release. With this aim, the near surface microstructure of different Ni-Ti wires is investigated by different transmission electron microscopy (TEM) techniques. The surface chemical composition of the wires and the elemental states of surface constituents were evaluated with the help of electron energy loss spectroscopy (EELS). High-resolution transmission electron microscopy (HRTEM) and energy filtered transmission electron microscopy (EFTEM) were used to obtain general information on elemental distribution from the surface layers to the bulk. In order to discriminate the type of Ni compound in the surface, energy loss near edge structure (ELNES) spectra were recorded.

## 2. Materials and methods

Four different commercial Ni-Ti wires with various surface oxide thickness were studied. The latter were determined before by TEM and are listed in Table 1 in increasing order together with some information on the materials preparation. Wires 1, 2 and 4 are classical Nitinol wires of 3 mm diameter straightened at 500°C under various levels of argon/oxygen atmosphere to produce varying oxide thickness [6,7]. Wire 4 is a so-called microwire, 30% cold-worked after wire drawing and has a nominal composition of Ti<sub>50.52</sub>Ni<sub>49.48</sub> [8]. More details on the treatment of the wires used in the present study can be found elsewhere, although, due to the commercial nature of the products, not all data on the relevant processes is available, unfortunately. [6,7,8].

<sup>a</sup> e-mail: he.tian@ua.ac.be

**Table 1:** TEM measures of the oxide layer thickness in view of materials processing data of the different wires

wire nb.	color of appearance	measured thickness oxide (by TEM; nm) [6,8]	treatment	diameter wire
1	violet - brown	30-50	500°C, argon/oxygen	3 mm
2	gold - brown	70-100	500°C, argon/oxygen	3 mm
3	dark grey - black	120-150	cold-worked	0.055 mm
4	dark blue - black	160-190	500°C, argon/oxygen	3 mm

The TEM specimens were prepared by site-specific focused ion beam using in-situ lift-out in an FEI FIB/SEM xT Nova Nanolab 200 [8] allowing for optimal sample thickness [9]. The conventional TEM studies were performed using a CM20 Philips instrument. The HRTEM imaging and EELS studies were conducted using an UltraTwin CM30 Philips FEG instrument equipped with a post-column GIF200 detector. High-angle annular dark field (HAADF) scanning TEM (STEM) experiments were performed using a JEOL 3000F TEM/STEM.

### 3. Results and discussion

The results of mixed EFTEM for nickel, titanium and oxygen are shown in Fig. 1a-d for all wires. These maps confirm that the surface layer predominantly consists of Ti and O. Additionally ELNES spectra (not shown here) reveal that the surface oxide of wires 3 and 4 is mostly  $\text{TiO}_2$  [8,10] while for the other two wires there is also a contribution from TiO. For example, in the case of wire 2, the bottom part of the oxide layer, i.e. closer to the alloy surface, reveals TiO, while the external layer is  $\text{TiO}_2$ . In wire 1, however, both oxide phases appear to be mixed, as becomes clear from the broadening in the ELNES [6]. The difference between these oxides is also obvious from the EFTEM map in Fig. 1, with a more homogeneous picture for wires 3 and 4 than for wires 1 and 2. More details on these recent EELS and ELNES spectra can be found elsewhere [6,8]

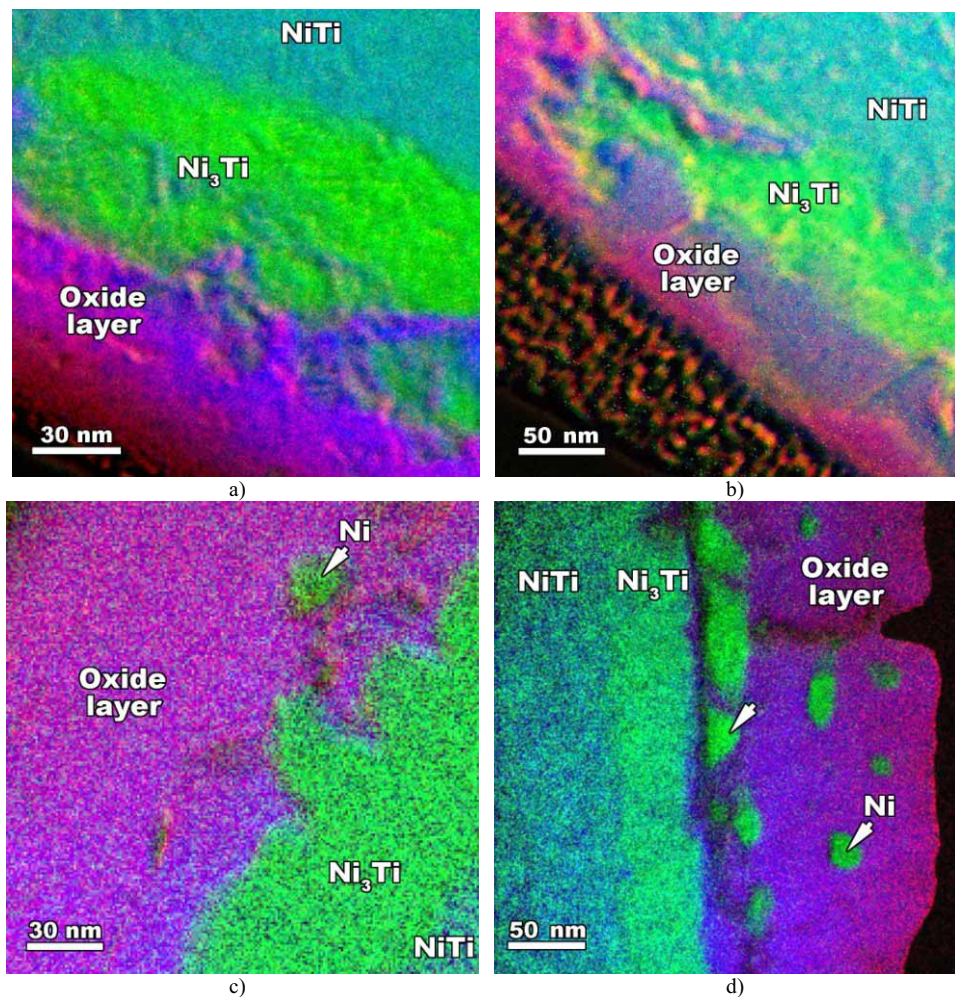


**Fig. 1.** Mixed EFTEM images for four wires 1 (a) to 4 (d). (red, blue and green indicate O, Ti and Ni elements, respectively. The arrows point at metallic Ni nanoparticles in wires 3 and 4)

Furthermore, an intermediate Ni-rich layer is present at the bulk-oxide interface with protrusions clearly matching the discontinuities in the oxide layer. This intermediate Ni-rich layer was identified as  $\text{Ni}_3\text{Ti}$  using energy dispersive X-ray (EDX) analysis as well as HRTEM. [6,8] The most important observation, relevant to the issue of Ni release, is the presence of Ni-rich nanoparticles embedded in the oxide layer and beginning from a surface depth of as low as 25 nm, as shown in Fig. 1 (c) and (d) for wires 3 and 4.

Since the Ni-rich nanoparticles are embedded in an oxide surface and surrounded by and sometimes overlapping with  $\text{TiO}_2$  and TiO grains, measuring their chemical composition and/or determining their type of Ni compound is not always straightforward. In order to identify the nature of the Ni-rich particles, ELNES of the Ni  $L_{2,3}$  edge from B2, B19',  $\text{Ni}_3\text{Ti}$  and the metallic Ni phase are compared in Fig. 2 (a). For the purpose of quantitative comparison, the spectra were normalized for Ni, after background subtraction and deconvolution with the corresponding low loss spectra. The  $L_3$  peak of Ni from metallic Ni is obviously higher than that from the other phases. Correspondingly, the Ni  $L_3$  peak from a Ni richer phase is expected to be higher than that from phases poorer in Ni. As the integrated intensity of the normalized ionization edges is proportional to the number of 3d holes, the number of 3d band electrons can be derived from the edge intensity [11]. The total amount of 3d electrons, i.e. the integrated intensity Ni  $L_3$ , can be considered as a parameter to distinguish various Ni compounds. Based on the intensity ratio of Ni  $L_3$  and  $L_2$  peaks in the ELNES from the present Ni-rich nanoparticles, the particles in the Ti-O surfaces are all but few identified as pure metallic Ni.

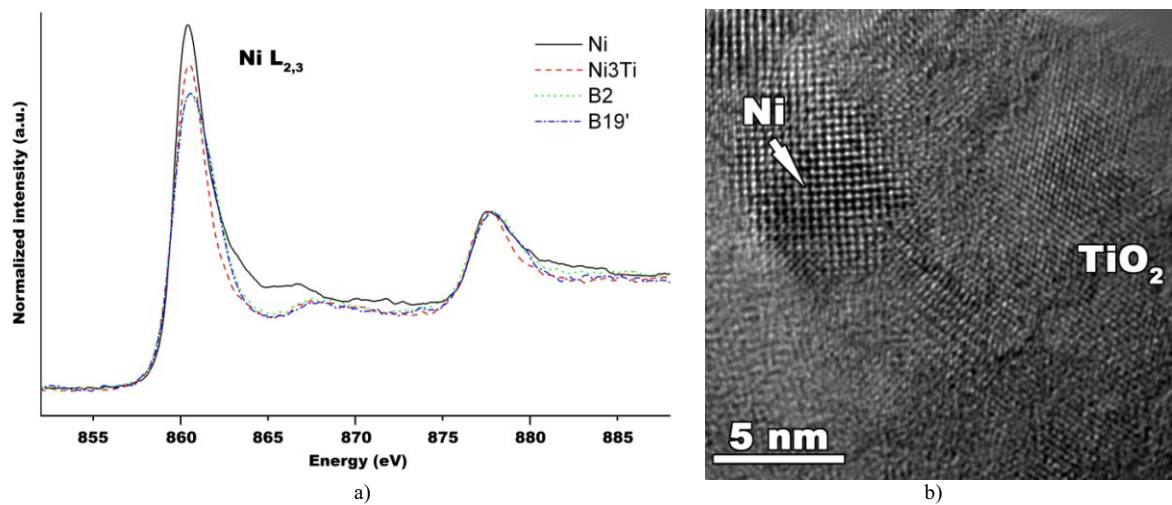


**Fig. 2.** (a) Comparison of ELNES of Ni L-edges from B2, B19',  $\text{Ni}_3\text{Ti}$  and metallic Ni phase; (b) HRTEM image of a metallic Ni nanoparticle and surrounding  $\text{TiO}_2$ . (Ni particle is indicated by white arrowhead)

The HRTEM in Fig. 2 (b) confirms that pure metallic Ni exists in the oxide surface. It should be mentioned that few  $\text{Ni}_3\text{Ti}$  particles can be found till up to 30nm from the  $\text{Ni}_3\text{Ti}$  interface layer. The distribution of particles is in agreement with EFTEM observations. As shown in Fig. 1 (c) and (d), the elemental maps indicate that metallic Ni is present in these particles, with sizes varying from 5 to 80 nm, and larger particles are located closer to the interface with the  $\text{Ni}_3\text{Ti}$  layer.

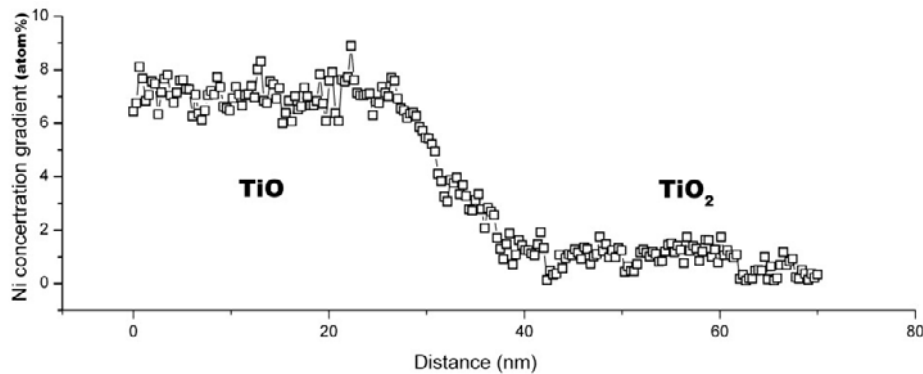


**Fig. 3.** Ni concentration profile that crosses the TiO and  $\text{TiO}_2$  parts of wire 2. The distance is measured away from the  $\text{Ni}_3\text{Ti}$  layer surface.

In contrast, no Ni nanoparticles can be seen in the surface layers of wires 1 and 2 in the EFTEM images in Fig. 1 (a) (b). Some Ni segregation can be seen in the bottom part of the oxide layer, i.e. the TiO part, of wire 2. Indeed, the Ni concentration profile obtained from the EFTEM shows a gradient of Ni distribution from the TiO towards the TiO<sub>2</sub>, as shown in Fig. 3. Obviously, the bottom TiO part contains more Ni atoms, up to 8 at.% as measured by EELS and EDX quantification. In fact, any Ni remains in the TiO<sub>2</sub> layer of wire 2 is hard to detect. From these observations it can be concluded that a Ti-oxide film with a higher degree of oxidation (Ti<sup>4+</sup>) facilitates not only the formation of metallic Ni particles, but also the reduction of the concentration of free Ni atoms.

It is important to clearly understand and quantify the size and distribution of Ni particles in the surface of these Nitinol wires. Using HAADF STEM, a Z-contrast technique producing an incoherent image, micrographs with a strong sensitivity to the atomic number can be obtained [12]. Therefore, regions containing the heavier atoms such as Ni (Z=28) and Ti (Z=22) will be imaged more bright, whereas the contrast from lighter atoms such as O (Z=8) can be negligible. In the HAADF STEM images, the metallic Ni particles with bright contrast can thus be easily recognized from the Ti-oxide background, as shown in Fig. 4. To get a better idea of the influence of the oxidation on the formation of Ni nanoparticles, the diameters of the metallic Ni particles have been measured from the HAADF STEM images. At least 30 particles in wires 3 and 4 were taken into account to allow a meaningful comparison. The corresponding schematic diagram of diameters of the Ni particles against the depth from the oxide surface to the oxide alloy interface is shown in Fig. 5 (a). When the depth of the particles increases, an exponential increase of the diameter of the Ni particles is observed. In the case of wire 4, beneath 150 nm from the surface, the size of particles increases more rapidly due to a layer consisting of larger Ni nanoparticles located close to the Ni<sub>3</sub>Ti layer, as shown in the upper half of the EFTEM of Fig. 1 (d). Furthermore, plenty of cracks appear in this area accompanying the Ni particles, as shown in both the EFTEM Fig. 1 (d) and HAADF STEM Fig. 4 (a) images.

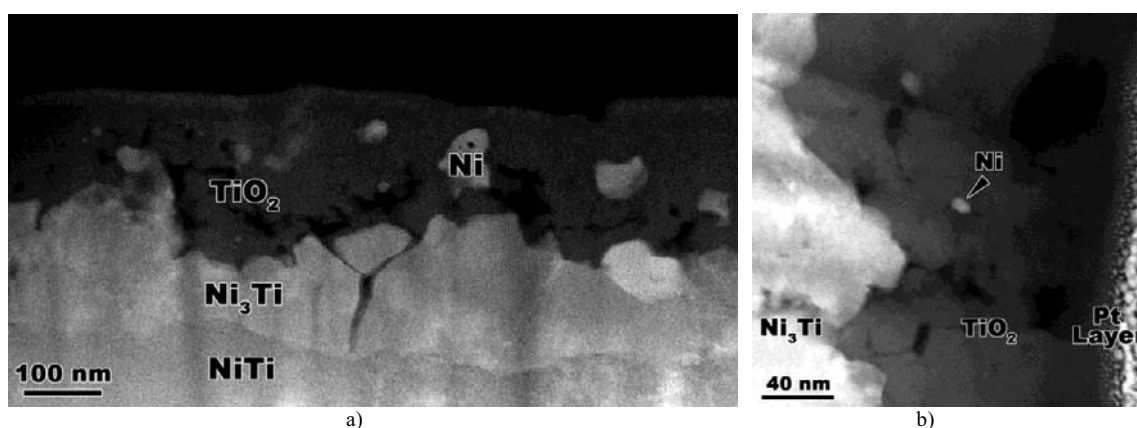


**Fig. 4.** The HAADF STEM images of a near surface area in wires 4 (a) and 3 (b).

In order to understand the influence of oxidation degree on the Ni release, an O/Ti ratio map was calculated based on the O and Ti EFTEM maps. In such a ratio map the effect of any thickness variations in the TEM sample are removed. For both wires 3 and 4, the quantified O/Ti ratio profile, based on EELS quantification as a reference, is shown in Fig. 5 (b). For wire 3 this ratio shows a gradual decrease of the degree of oxidation from the surface to the inside of the oxide layer. Correspondingly, the diameter of the Ni particles shows a linear increase. In wire 4, beneath 150 nm from the surface, the O/Ti ratio remains constant at approximately 1.4. At this depth, which is close to the interface with the bulk, large numbers of metallic Ni particles with large sizes can be found in the oxide layer. The size versus depth function now becomes exponential, with the possibility that the above linear part could be fitted to the first part of the same exponential function. This fact that Ni particles, whose number and size increase while approaching the interface between the surface and the bulk, indicates that the oxidation is the major driver force to form a Ni free layer on the outer surface. It should also be mentioned that the release of Ni from wire 4 exceeds that from other wires by a factor of at least 100 [6]. This can be ascribed to the existence of many cracks in the thick oxide layer in wire 4 reaching all the way down to the Ni<sub>3</sub>Ti interface layer yielding a Ni<sub>3</sub>Ti layer exposed to the surrounding environment.

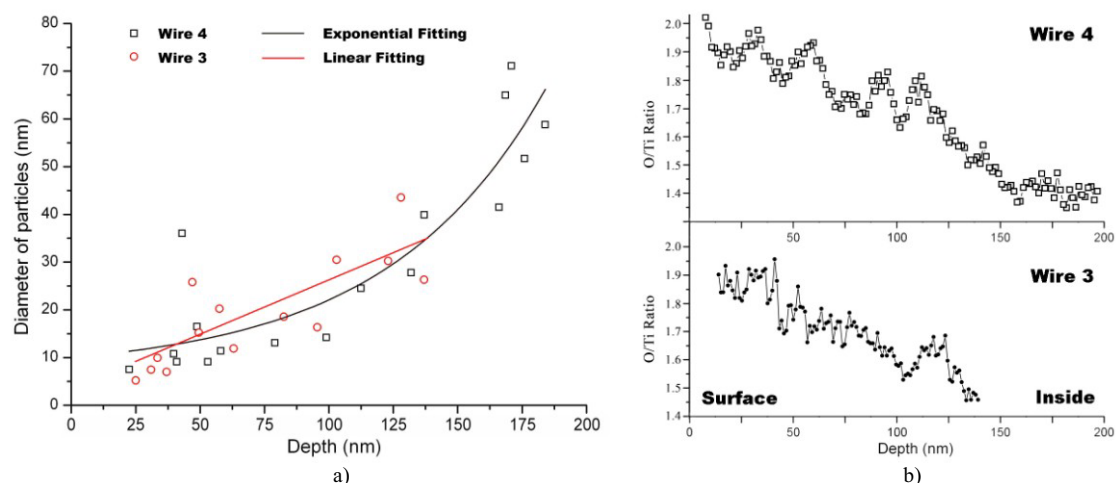


**Fig. 5.** (a) Schematic diagram of particle diameter against the depth of distribution from surface to inside (linear and exponential fittings are included); (b) O/Ti ratio profile in the oxide surface of wires 3 and 4.

Preliminary results of molecular dynamics calculations reveal that a pure Ni nanoparticle has a lower energy than free Ni atoms inside the  $\text{TiO}_2$  lattice. Indeed, the bonding energy at  $T = 0\text{K}$  of two Ni atoms in  $2 \times 2 \times 3$  unit cells of  $\text{TiO}_2$  (rutile) is calculated by the method of DMol 3 [13] after geometric optimization, as shown in the schematic of Fig. 6 (a). Fig. 6 (b) shows the structural model of 2 bonded Ni atoms in the rutile lattice after geometric optimization (one Ni atom occupies the position of an O, the other occupies the position of a Ti before optimization). The results show that Ni atoms tend to bond together to form a metallic particle that is more stable compared with the case of free Ni atoms. The calculated results are in agreement with the experimental observations mentioned above. Larger sizes of particles reduce the probability of Ni diffusion from the oxide surface to the surrounding tissue of the human body.

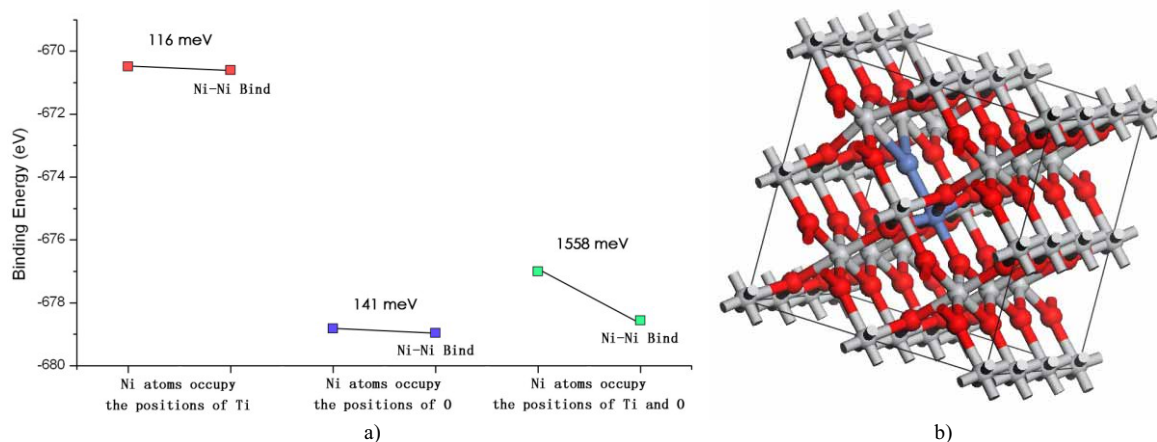


**Fig. 6.** (a) Schematic diagram of binding energy with different types of occupation position of a Ni atom in a  $\text{TiO}_2$  lattice; (b) schematic image of structural model of 2 bonded Ni atoms in a  $\text{TiO}_2$  rutile lattice after geometric optimization. (blue indicates Ni atom, red O and white Ti)

From the present study it can thus be concluded that the Ni release is dominated by metallic Ni particles rather than Ni atoms. These results also imply that by properly controlling the thickness and oxidation state of the outer  $\text{TiO}_2$  layer, restricting Ni release is effectively feasible.

### 3. Conclusions

The present study demonstrates that by properly controlling the oxide surface layer and especially its degree of oxidation, one may be able to decrease or even avoid Ni release. In the case of violet to gold shining wires 1 and 2 with an oxide thickness below 100nm, the bottom part of the oxide surface layer with a lower oxidation degree ( $\text{Ti}^{+2}$ ) is mostly  $\text{TiO}$ . A higher density of free Ni atoms in such a layer is a potential source of Ni release. Further oxidation from  $\text{TiO}$  to  $\text{TiO}_2$  will allow more stable Ni particles to be formed from these free Ni atoms. In the case of wire 4, in the thicker oxide surface layer with increased oxidation, the size of metallic Ni particles rapidly

increases while approaching the interface between the surface and the bulk. Also close to cracks in the oxide layer, Ni particles close to the Ni<sub>3</sub>Ti layer are often observed possibly due to galvanic corrosion from penetrating liquids.

Support for this work was provided by the FWO projects G.0576.09N “Three-dimensional characterization of precipitates in Ni-Ti shape memory alloys by slice-and-view in a FIB-SEM dual-beam microscope” and G.0180.08 “Optimization of Focused Ion Beam (FIB) sample preparation for transmission electron microscopy of alloys”.

## References

- [1] K.W.K. Yeung, R.W.Y. Poon, X.Y. Liu, J.P.Y. Ho, C.Y. Chung, P.K. Chu, W.W. Lu, D. Chan, K.M.C. Cheung, *J. Biomed. Mater. Res.* **75A** (2005) 256–267
- [2] O. Cisse, O. Savagodo, M. Wu, L. Yahia, *Biomed. J. Mater. Res.* **61** (2002) 339–345
- [3] S. Kobayashi, Y. Ohgoe, K. Ozeki, K. Sato, T. Sumiya, K. Hirakuri, *Diamond Related Mater.* **14** (2005) 1094–1097
- [4] J. Sui, W. Cai, *Diamond Related Mater.* **15** (2006) 1720–1726
- [5] B. Clarke, W. Carroll, Y. Rochev, M. Hynes, D. Bradley, D. Plumley, *J. Biomed. Mater. Res.* **79A** (2006) 61–70
- [6] S.A. Shabalovskaya, H. Tian, J.W. Anderegge, D. Schryvers, W.U. Carrol, J. Van Humbeeck, *Biomaterials*, **30** (2009) 468–477
- [7] B. Clarke, P. Kingshott, X. Hou, Y. Rochev, A. Gorelov, W. Carroll, *Acta Biomater* **3** (2007) 103–111
- [8] H. Tian, D. Schryvers, S.A. Shabalovskaya, J. Van Humbeeck, *Microscopy and Microanalysis*, **15** (2009) 62–70
- [9] S. Bals, W. Tirry, R. Geurts, Z. Yang, D. Schryvers, *Microsc. Microanal.* **13** (2007) 80–86
- [10] R. Brydson, H. Sauer, W. Engel, J.M. Thomas, E. Zeiter, N. Kosugi, H. Kuroba, *J. Phys.: Condens. Matter* **1** (1989) 797–812
- [11] Z.L. Zhang, W. Sigle, W. Kurtz, M. Rühle, *Phys. Rev. B* **66** (2002) 214112
- [12] P.D. Nellist, S.J. Pennycook, *Ultramicroscopy* **78** (1999) 111–124
- [13] B. Delley, *J. Chem. Phys.* **113** (2000) 7756–7764